

Joint Use of EGMS and Cosmo-SkyMed InSAR for Assessment of Ground and Structural Deformations: The Case of Como, Northern Italy

Rasoul ESKANDARI^{1,*}, and Marco SCAIONI¹

¹Dept. of Architecture, Built Environment and Construction Engineering, Politecnico di Milano, Milano, Italy
(rasoul.eskandari@polimi.it, marco.scaioni@polimi.it)

*corresponding author

Abstract

Urban ground deformation poses significant risks to structural stability and infrastructure resilience, necessitating advanced monitoring techniques. This study evaluates two critical structural deformation parameters—maximum lowering rate and maximum differential settlement—using Interferometric Synthetic Aperture Radar (InSAR) measurements from COSMO-SkyMed (CSK) and Sentinel-1 (EGMS Level 2b) datasets in Como town, Northern Italy, over the period January 2016 to December 2021. CSK data were processed using Multi-Temporal InSAR (MT-InSAR) techniques, while Sentinel-1 deformation velocities were extracted directly from the European Ground Motion Service (EGMS) portal. A specific geospatial approach was employed to mitigate the impact of localized deformations and simplify single-building analyses without requiring computationally intensive processing steps. The comparison between CSK and EGMS datasets revealed a reasonable level of agreement, demonstrating their complementary strengths in deformation monitoring. Results indicate that 33 buildings were subject to significant lowering rates, while 99 buildings exhibited notable differential settlement. These findings underscore the utility of integrating high-resolution datasets for comprehensive urban deformation assessments. This research contributes to the growing body of knowledge on urban geohazard assessment by highlighting the efficacy of InSAR technologies in structural condition monitoring. The insights gained from this study are expected to inform future applications of InSAR for structural and infrastructure condition assessment and monitoring.

Keywords: Structural Monitoring, InSAR, EGMS, Cosmo-SkyMed, Como

Received: 9th December 2024. Revised: 24th February 2025. Accepted: 24th February 2025.

1 Introduction

Monitoring ground deformation in urban areas is crucial for assessing structural stability and mitigating geohazards. Interferometric Synthetic Aperture Radar (InSAR) has emerged as a pivotal technology in this domain, enabling precise measurements (millimetric-level accuracy) of surface displacements over extensive regions. The applicability, reliability and efficiency of InSAR technique in different fields of application, such as detecting subsidence, landslides, and infrastructure deformations have been well-documented through literature (Solari et al., 2020; Raspini et al., 2022).

The European Ground Motion Service (EGMS), as valuable service offered by Copernicus Land

Monitoring Service (CLMS), provides standardized ground motion data across Europe, utilizing Sentinel-1 satellite imagery to deliver consistent and accessible deformation measurements. Complementing this, the COSMO-SkyMed (CSK) constellation offers high-resolution SAR data, facilitating detailed analyses of localized deformation phenomena. The integration of EGMS and CSK datasets enhances the capability to monitor and interpret ground deformation dynamics effectively (Gagliardi et al., 2021), especially when single-building condition assessment is concerned.

Como town, located adjacent to Como Lake at the north of Italy, is well-known in terms of considerable subsidence rates over the last decades. Passing from traditional geodetic measurements,

InSAR has been used through different studies to measure and monitor different rates of subsidence over this area (Nappo et al., 2020; Eskandari, 2022).

Building upon this foundation, the present study aims to evaluate deformation parameters—specifically maximum lowering and maximum differential settlement—using both EGMS Level 2b and CSK InSAR measurements. By comparing these datasets, the study seeks to elucidate their respective responses and accuracies in capturing deformation characteristics in Como. For the detection of both parameters, a specific approach has been used to suppress the effect of extremely local deformations on the results for each building, and not to apply high-demanding processing steps in single-building analyses.

This research contributes to the existing body of knowledge by providing an integrative and comparative analysis of EGMS and CSK datasets in urban deformation monitoring. The findings are expected to inform future applications of InSAR technology in structural and infrastructure deformation monitoring.

2 Material

The Area of Interest (AoI) in this study is Como town and surrounding, up to Sagnino at the northwest and Camerlata at the south, as depicted in Figure. 1. The Reference Point (RP) for all displacement measurements is also indicated in Figure 1, signifying that all measurements are referenced to this location.

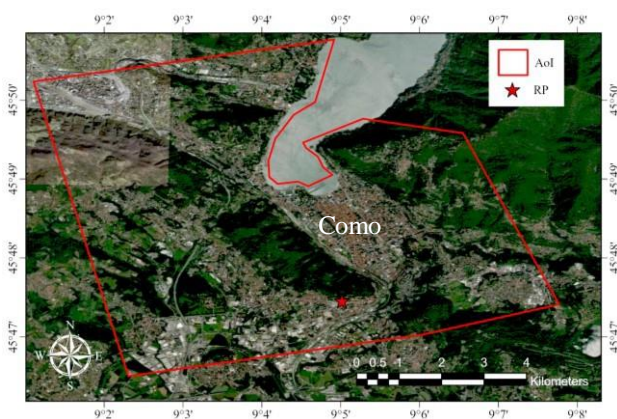


Figure 1. Area of Interest (AoI) and Reference Point (RP) for deformation measurements.

To reach the purpose of this study, two sources of ground displacement information have been used which are: *i*) obtained by MT-DInSAR applied to 95 Single-Look Complex (SLC) Cosmo-SkyMed (CSK) SAR images, and *ii*) extracted from European

Ground Motion Service (EGMS) portal (based on MT-DInSAR processing of Sentinel-1 SAR images). Basic properties of both types of SAR images are provided in Table 1.

Table 1. Properties of Cosmo-SkyMed (CSK) and Sentinel-1 (used in EGMS) SAR images

Property	CSK	Sentinel-1 (EGMS L2b)
Orbit Track	Ascending	Ascending
Incident Angle [°]	28.94	37.19
Acquisition Mode	StripMap - HIMAGE	Interferometric Wide Swath
Resolution [~m]	Az 3 × Rg 3	Az 20 × Rg 5
Temporal Coverage	Jan 2016 – Dec 2021	Jan 2016 – Dec 2021

The CSK images have undergone a processing chain to obtain ground deformations, which will be described in the next section; however, the ground deformations from Sentinel-1 are directly extracted from the EGMS portal which is discussed in the following sub-section.

2.1. European Ground Motion Service

As a sector of Copernicus Land Monitoring Service (CLMS), EGMS offers valuable datasets of ground deformation with pan-European spatial coverage, using European Space Agency (ESA) Sentinel-1 SAR images. The deformation time-series provided by the service take advantage of a nominal temporal resolution of 6 days (until the Sentinel-1B failure in Dec 2021) and 12 days (after the incidence), however, the spatial resolution is tied to the level of product, which are outlined in Table 2 (Crosetto et al., 2020). The EGMS products and their effectiveness in different fields of application have been evaluated through literature (Eskandari and Scaioni, 2023; Crosetto and Solari, 2023; Cuervas-Mons et al., 2024; Eskandari and Scaioni, 2024).

It should be noted that deformations in L2A products are relative to a local reference point, however, the other two types are derived from calibration with Global Navigation Satellite System (GNSS) measurements and there is no local reference point for these deformations. In this work, the L2b (of ascending track dataset) and the L3 (of East-West and Up-Down datasets) products of EGMS covering the AoI are exploited. The data are freely accessible through the portal (www.egms.land.copernicus.eu).

Table 2. EGMS product levels and the properties

Product	Spatial Res.	Direction of Deform.
L2A - BASIC	Sentinel-1 Pixels	LOS of: Ascend. and Desc.
L2B - CALIB	Sentinel-1 Pixels	LOS of: Ascend. and Desc.
L3 - ORTHO	100 m	Esat-West and Up-Down

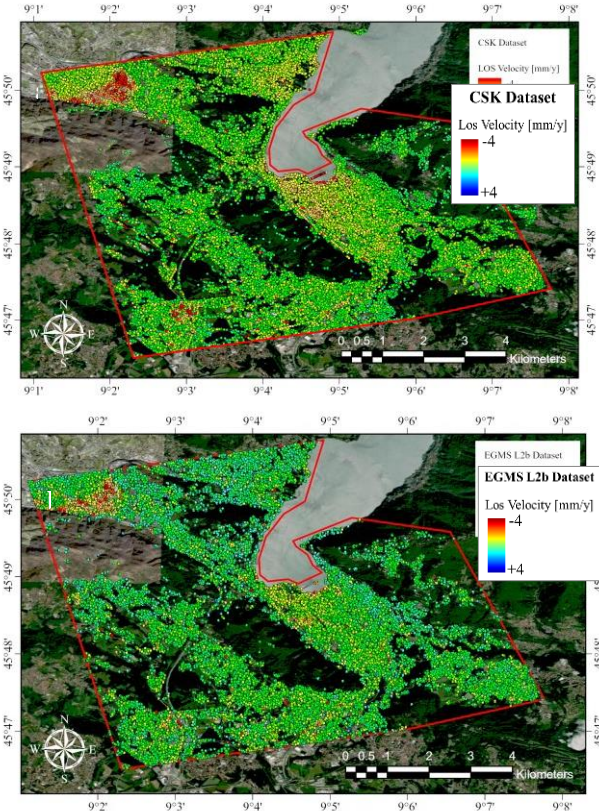


Figure 2. Data points colored with LOS displacement velocity exploited from: a) Cosmo-SkyMed (ascending), and b) EGMS L2b (Sentinel-1 ascending).

2.2 Building Polygons

In order to assess the single-building condition of deformation, the building polygons of all the buildings in AoI have been extracted from Geoportal of Lombardy Region. These geospatial data are included in the Geo-Topographic Database (DBGT), available at www.geoportale.regione.lombardia.it.

3 Methodology

3.1 CSK MT-DInSAR Processing

In order to obtain deformation velocities over the scene using CSK images, 95 images (spanning from Jan 2016 to Dec 2021) acquired in ascending track

have been exploited through SAPROZ software (Perissin et al., 2011). First, the images have been cropped according to AoI, and then, have been co-registered. After the calculation of spatial coherence through a full-graph configuration among the images, the best possible connections (in terms of high spatial coherence) among images are selected to establish a Minimum Spanning Tree (MST) configuration, based on which the mean spatial coherence $Coher_{spt}$ (in the range of $[0, 1]$) for each pixel in the scene has been calculated. Furthermore, the Amplitude Stability Index is also calculated for all the pixels. This measure can be obtained for each pixel as $Idx_{AmpStab} = 1 - \sigma_A / \mu_A$, where σ_A and μ_A represent the standard deviation and mean of the amplitude time-series of the corresponding pixel. Similar to well-known Amplitude Dispersion, this parameter which varies in the range of $[-Inf, 1]$ quantifies how stable or reliable the amplitude remains over time. By thresholding the sum of these two parameters representing pixel quality (Eskandari, 2022):

$$Coher_{spt} + Idx_{AmpStab} \geq 1 \quad (1)$$

the Persistent Scatterer Candidates (PSCs) have been selected for MT-DInSAR processing. Atmosphere delay is one of the most challenging contributions involved in DInSAR for such processing, which should be properly estimated and removed from each interferogram, so it will not affect the InSAR deformation measurements. The module of Atmosphere Estimation in the software has been used, through which the Delaunay triangulation is established among a portion of PSCs selected in the previous step to estimate the atmosphere-related phase differences in a single-master configuration among images. A pixel as the global reference point is also selected in this step (close to the Reference Point (RP) shown in Fig. 1), which gives all the measurements relative to this pixel (readers seeking further information are encouraged to refer to (Eskandari, 2022)).

After the estimation of atmospheric phase screens, which also includes a significant portion of noise expected, this contribution is removed from each interferogram, and the set of atmospheric-corrected interferograms are ready for MT-DInSAR processing. Considering a single-master configuration, Equation 2 is solved for each PSC to obtain deformation velocity (Eskandari, 2022):

$$\Delta\varphi_i = \mathbf{K}_{\Delta H} \Delta H + \mathbf{K}_{\Delta V} \Delta V + \mathbf{K}_{\Delta T} \Delta T + \mathbf{n} \quad (2)$$

where $\Delta\varphi_i$ is the vector of double differential phases

(temporal differential with respect to the master image and spatial differential with respect to the reference point) of i^{th} PSC and \mathbf{n} is the remaining inevitable noise; $\mathbf{K}_{\Delta H}$, $\mathbf{K}_{\Delta V}$, and $\mathbf{K}_{\Delta T}$ are known vectors proportional to vectors of β_{prep} (perpendicular baseline), $\beta_{temporal}$ (temporal baseline) and β_{therm} (thermal baseline, i.e., the temperature of the scene at the slave acquisitions with respect to the master acquisition, extracted from www.virtualcrossing.com), respectively. The unknown variables to be estimated are: ΔH residual height of the target with respect to the used DEM for flattening the interferograms, ΔV deformation velocity of the target along the Line of Sight (LOS) of the satellite, and ΔT deformation rate with respect to the temperature variations.

After fitting a model and defining these unknown variables, the quality of the model can be quantified using temporal (or multi-acquisition) coherence $Coher_{tmp}$ (ranging in the interval of [0 1], with 1 as the best possible fit). In this study, after processing all the PSCs, the ones with $Coher_{tmp} \geq 0.7$ are chosen as the final PSs representing the deformation of the scene. The final result, in terms of CSK LOS displacement velocity, is depicted in Figure 2(a).

3.2 Compensation and Projection

To perform MT-InSAR and obtain ground displacement information, it is essential to consider a Reference Point (RP), and in this way, all the deformation measurements are with respect to this RP. Since each dataset has its own RP, it is necessary to have the displacement information with respect to a common RP for both CSK and EGMS datasets, in order to allow for comparison. Here, the CSK-derived deformations are already obtained with respect to the RP indicated in Fig. 1. On the Other hand, The EGMS Calibrated data used in this study are referenced to the Earth's centre of mass and aligned with the WGS84 coordinate system, which defines both the origin and orientation (due to being calibrated with GNSS measurements). Therefore, a point in the vicinity of the RP is chosen, and all the displacement velocities are compensated with respect to this point. In this way, more comprehensible datasets (from both CSK and EGMS) are provided for the purpose of this study.

Both the CSK- and EGMS-derived deformation datasets are in their corresponding LOS direction, with a slight difference (see incident angles in Table 1). To make the measurements comparable, it is necessary to take the common direction of deformations.

It should be noted that, due to the near-polar orbits of the SAR satellites, the InSAR measurements are insensitive (or with low sensitivity) to deformations along the North-South Direction (Mehrabi et al., 2019); therefore, there are two components, if the presence, contributing in the magnitude of LOS measurements: vertical up-down (U-D) and horizontal east-west (E-W) deformations. Taking a look at the E-W deformations provided by EGMS Ortho (L3) products over the AoI of this work, it can be observed that the magnitude of deformations in this horizontal direction is not significant: mostly close-to-zero (this data are not presented in this paper to maintain its conciseness and focus). Assuming that the LOS deformations over the AoI are due to the vertical displacements, the LOS velocity of each dataset is converted to vertical U-D deformations by:

$$\Delta V_{vert} = \Delta V_{LOS} / \cos(\theta) \quad (3)$$

where θ indicates the incident angle of the satellite during the acquisition of that specific pixel. Here, the constant mean incident angle of each dataset is used for the vertical projection of deformation velocities.

3.3 Single-Building Analysis

To perform the single-building assessment, two deformation parameters are considered for each building in this study: Maximum Lowering Rate, Max_{Lower} and Maximum Differential Displacement Max_{Diff} . The main idea is to measure the minimum vertical velocity (Max_{Lower}) and the difference between the minimum and maximum velocities (Max_{Diff}) observed over each building. However, if a point-wise approach is adopted, the analysis may be affected by very extreme local processes over the building. On the other hand, interpolating the velocities and computing the gradient of the velocity in a pixel-wise approach may also indicate the extreme local processes. In this study, an approach is adopted in a way that these extreme local processes are suppressed as much as possible; so, using the data extracted for the whole AoI:

- Each building polygon is extended by a unique value (here, a 2-meter extension on each side) to consider the uncertainty of the PSs positioning.
- For each dataset of CSK and EGMS, the data points fallen into the extended building polygon are detected, and then, the values of linear velocities are interpolated using Inverse Distance Weighted (IDW) interpolation method over a uniform 2-meter grid defined over the

polygon.

- Maximum and Minimum velocities observed over the uniform grid are selected, and a buffer of 5-meter diameter is defined over each of these interpolated points detected as extremum values. Although the spatial resolutions of the two datasets are different, the deformation velocities have been interpolated over the same uniform grid, and this is the reason for choosing the same 5-meter buffer for both datasets.
- Max_{Poly} and Min_{Poly} are calculated as the average of the velocities observed in each corresponding buffer, and the maximum subsidence rate and maximum differential velocities are obtained by:

$$Max_{Low} = Min_{Poly} \quad (4)$$

$$Max_{Diff} = Max_{Poly} - Min_{Poly} \quad (5)$$

Following this approach, it is tried to suppress the extreme local values of velocities over each building. At the end, each building is assigned two deformation parameters, indicating the status of the building considering the whole duration of the assessment (2016-2021). It is also worth mentioning that the data points with a height lower than the height of the corresponding building are not removed in this study, since it is assumed that the data points lower than the height of the building, positioned on the lateral walls or in the close vicinity of the building on the ground, are also representative of the vertical velocity of the building. Furthermore, the buildings with an area smaller than $Thresh_{Area} = 40 \text{ m}^2$ or being characterized by the number of PSs (from each dataset) lower than 5 are filtered out from the analysis. In the next section, the overall results of the analyses, and the comparison and integration of CSK- and EGMS-derived information are provided.

4 Results and Discussion

4.1 Exploited Data Interpretation

The data that have been used in this work are two sources of ground deformation data and building polygons, all corresponding to AoI. Before going into the details of the final outcomes, it is beneficial to examine the overall stat of these data.

From 13,280 polygons (individual buildings), 12,440 polygons had area more than $Thresh_{Area} = 40 \text{ m}^2$. Very big polygons with up to approx. 22000 m^2 can be seen within the AoI, which are expected to be a suitable home for several PSs.

After thresholding the temporal coherence and removing the PSs with the values of temporal coherence lower than 0.7, the number of PSs

available from CSK and EGMS L2b are approx. 96700 and 70500, respectively. In terms of the magnitude of deformations, both Figure 1 (a) and (b) show a consistent spatial pattern of deformations over the AoI: getting away from satellite (i.e., subsidence) at lakeshore, north-west and south-west of AoI. It is worth mentioning that the highest subsidence rates of -13.2 and -9.9 [mm/y] , and uplift rates of $+5.5$ and $+7.2 \text{ [mm/y]}$ were observed over the AoI, respectively from CSK and EGMS datasets.

4.2 Feasibility for Structural Monitoring

As mentioned in Section 3, the buildings which contain at least 5 PSs are selected as the buildings on which the InSAR monitoring is possible. After performing the single-building analysis considering this criterion, the number of suitable buildings was observed to be 3,790 and 2,379, considering CSK and EGMS respectively. Following the lower spatial resolution of EGMS data points with respect to CSK, it was already expected that a smaller number of buildings could be assessed by EGMS data points. However, in a few cases, the data points from EGMS were sufficiently available whereas the CSK data points were not sufficiently found for structural monitoring.

4.3 Single-Building Results

Following the steps described in subsection 3.3, the most intense lowering rate and the maximum differential displacement of the buildings are obtained using both CSK and EGMS datasets. Fig. 3 and Fig. 4 show some examples with the CSK and EGMS L2b, respectively, the data points over this small area. Since the variation of both deformation parameters is not very significant, they have been grouped into only two categories: for maximum lowering the values of displacement velocity lower than -2.5 [mm/y] are considered as considerable (red polygons), and for maximum differential displacement, the values higher than 2.5 [mm/y] are considered as considerable (red polygons). The thresholds are chosen based on practical interpretation and pragmatic considerations, taking into account the 3σ range of the displacement rates.

The first initial observation is that the locations with negative values of velocities in the EGMS dataset show more or less the same pattern as CSK data points (Fig. 3 (a) and Fig 4 (a)). Furthermore, a notable agreement can be witnessed between the detected categories for both

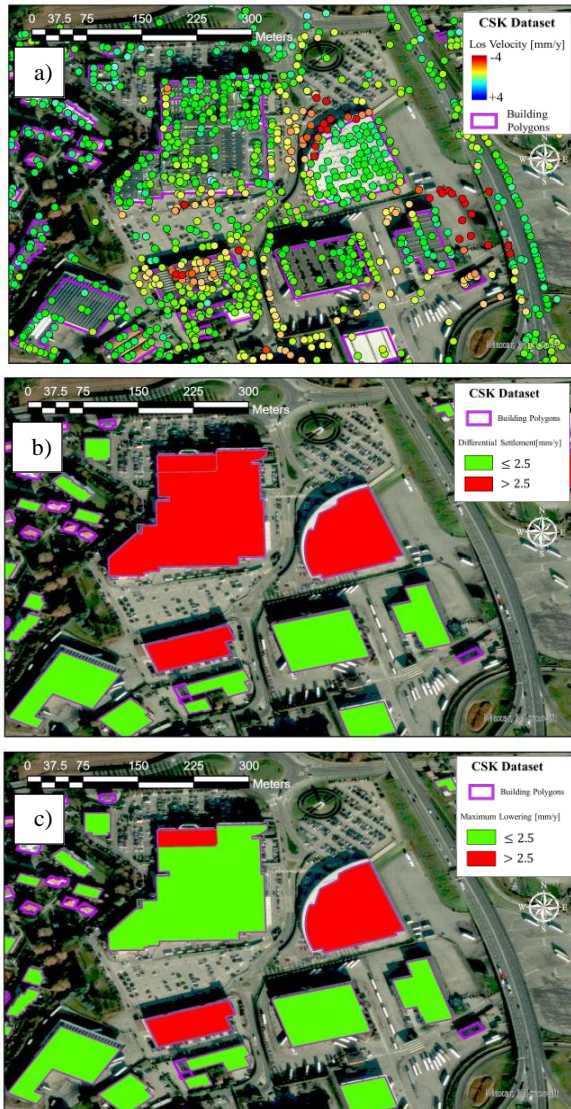


Figure 3. Example of a small area with a) building polygons and CSK data points, b) and c) the detected differential settlement and maximum lowering, respectively.

deformation parameters; Except for the large building in the middle of this small area that shows a green situation in terms of maximum lowering. Some evaluated small buildings (all green) are present in Fig. 3 which are not inspectable by the EGMS dataset and are not illustrated in Fig. 4, which again shows the privilege of using high-resolution InSAR for structural condition assessment.

Such analysis and comparison can be done for the whole area, however, here, only one example is shown to clarify the results. Although a reasonable match has been seen in the example small area discussed above, it is crucial to also evaluate the CSK-EGMS match all over the area. Fig. 5 shows the difference between CSK- and EGMS-derived

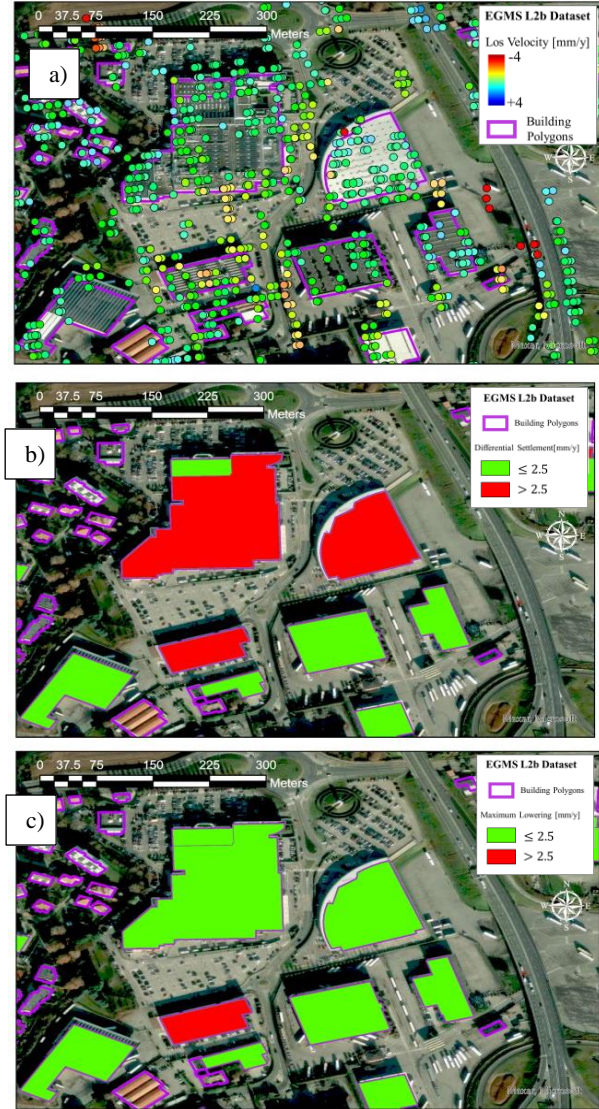


Figure 4. Example of a small area with a) building polygons and EGMS L2b data points, b) and c) the detected differential settlement and maximum lowering, respectively.

deformation parameters through single-building analysis, where high and low values are two categories for each parameter (discussed above). As can be seen, a large portion of buildings show a low status in both parameters. For the rest, in terms of maximum lowering, CSK measurements show more conservative values, rather than EGMS; however, the differential settlements over the AoI obtained by EGMS data show more conservative measures than CSK data.

This mismatch can be due to a varying set of reasons, such as the setting of the threshold for high-low category assignment to each building, computational errors and inconsistencies for processing of each dataset, different numbers of available points for each building, etc. Although it

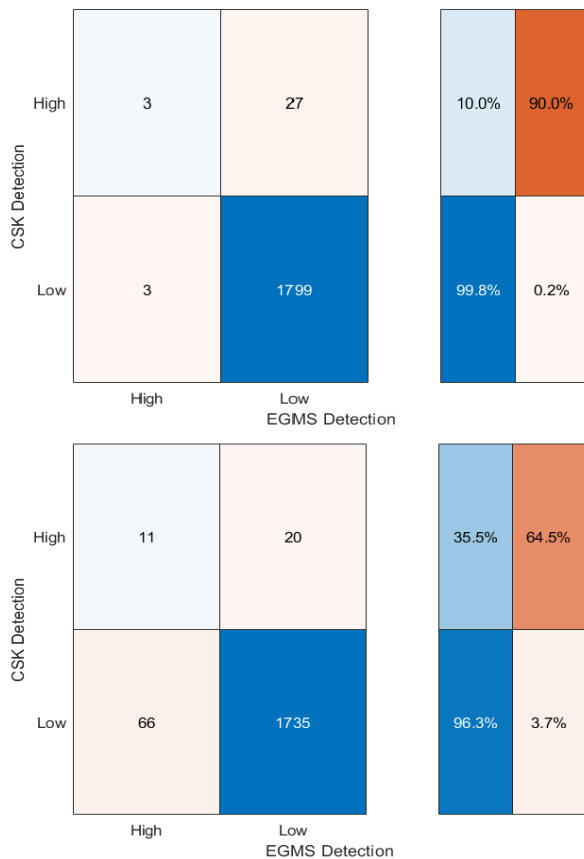


Figure 5. Label agreement matrix for comparing CSK- and EGMS-derived deformation parameters through single-building analysis: maximum lowering (above) and differential settlement (below).

is out of the scope of the current study, unfortunately, there is no precise and/or ground-truth data available at the current state for validation of displacement information (data such as geodetic leveling and GNSS measurements), validation of classification performed in this work (such as building damage data), and assessing the cause of the intense deformations (data such as groundwater variations). Here, only a cross-sensor check and a multi-sensor integration have been performed on the use of InSAR for the structural condition assessment. The integration of InSAR with other sources of information through a multi-disciplinary approach (Scaioni et al., 2025) will be the perspective for future studies.

Nonetheless, to integrate the use of EGMS L2b and CSK measurements, the most conservative observation from each dataset can be considered as the final condition of each building. In this way, the number of 33 and 97 buildings can be reported to be imposed by significant lowering rates and differential settlements over the whole of AoI.

5 Conclusion

This work is intended to assess the building condition in terms of maximum lowering rate and differential settlement, two important structural deformation parameters, using InSAR measurements using Cosmo-SkyMed and Sentinel-1 (EGMS L2b) SAR images over Como town, Italy, in the period of Jan 2016 to Dec 2021. The CSK images have been processed through MT-InSAR to obtain displacement velocities over the area, however, the deformation velocities from Sentinel-1 have been extracted directly from the EGMS portal. The single-building (using geospatial data: building polygons) analysis has been performed through a specific approach to tackle the effect of extremely local deformations detected by InSAR technology over the building under study. A comprehensive comparison between the CSK- and EGMS-derived information showed a reasonable agreement between the datasets. It has been observed that, after integrating both datasets, 33 buildings were affected by considerable lowering rates, and 99 buildings suffered from significant values of differential settlement.

References

- Crosetto, M., Solari, L., 2023: Satellite Interferometry Data Interpretation and Exploitation: Case Studies from the European Ground Motion Service (EGMS). Elsevier.
- Crosetto, M., Solari, L., Balasis-Levinsen, J., Casagli, N., Frei, M., Oyen, A., Moldestad, D. A., 2020. Ground deformation monitoring at continental scale: the European ground motion service. *The International Archives of Photogrammetry, Remote Sensing and Spatial Information Sciences*, 43, 293-298.
- Cuervas-Mons, J., Domínguez-Cuesta, M. J., Jiménez-Sánchez, M., 2024. Potential and Limitations of the New European Ground Motion Service in Landslides at a Local Scale, 14(17), 7796.
- Eskandari, R., 2022. Retrospective study of subsidence in Como town: integration of levelling measurements, DInSAR, and geospatial techniques. MSc thesis at Politecnico di Milano on civil Eng. for Risk Management, Lecco Campus (available at <https://hdl.handle.net/10589/195212>).

- Eskandari, R., Scaioni, M., 2023. European Ground Motion Service For Bridge Monitoring: Temporal And Thermal Deformation Cross-Check Using Cosmo-SkyMed InSAR.
- Int. Arch. Photogramm. Remote Sens. Spatial Inf. Sci., XLVIII-1/W2-2023, 1235-1241.
- Eskandari, R., Scaioni, M., 2024. Spatiotemporal Pattern Detection of Ground Deformations Induced by Extreme Rainfall using InSAR EGMS: The case of Cortina d'Ampezzo after Vaia Storm. ISPRS Ann. Photogramm. Remote Sens. Spatial Inf. Sci., X-3-2024, 131-138.
- Gagliardi, V., Ciampoli, L. B., Amico, F. D., Alani, A. M., Tosti, F., Battagliere, M. L., Benedetto, A., 2021. Novel Perspectives in the Monitoring of Transport Infrastructures by Sentinel-1 and Cosmo-SkyMed Multi-Temporal SAR Interferometry. 2021 IEEE International Geoscience and Remote Sensing Symposium IGARSS, 1891-1894.
- Mehrabi, H., Voosoghi, B., Motagh, M., Hanssen Ramon, F., 2019. Three-Dimensional Displacement Fields from InSAR through Tikhonov Regularization and Least-Squares Variance Component Estimation. Journal of Surveying Engineering, 145(4), 04019011.
- Nappo, N., Ferrario, M. F., Livio, F., Michetti, A. M., 2020. Regression Analysis of Subsidence in the Como Basin (Northern Italy): New Insights on Natural and Anthropogenic Drivers from InSAR Data. 12(18), 2931.
- Perissin, D., Wang, Z., Wang, T. J. P. o. t. I., Sidney, Australia, 2011. The SARPROZ InSAR tool for urban subsidence/manmade structure stability monitoring in China. 1015.
- Raspini, F., Caleca, F., Del Soldato, M., Festa, D., Confuorto, P., Bianchini, S., 2022. Review of satellite radar interferometry for subsidence analysis. Earth-Science Reviews, 235, 104239.
- Scaioni, M., Eskandari, R., Garramone, M., Barindelli, S., Galli, A., Realini, E., Sansò, F., Ravasi, D., Aghemio, M., Lucidera, L., and Sciannamé, S., 2025. HeMOC: a Project to Develop a Multisensor Network for Monitoring Historical Cities. In: Proc. 23. Int. Geodätische Woche, 9-15 February 2025, Obergurgl (Tyrol, Austria).
- Solari, L., Del Soldato, M., Raspini, F., Barra, A., Bianchini, S., Confuorto, P., Casagli, N., Crosetto,
- M., 2020. Review of Satellite Interferometry for Landslide Detection in Italy. Remote Sensing, 12(8), 1351.